JCTC Journal of Chemical Theory and Computation

Article

pubs.acs.org/JCTC

Computing the Role of Near Attack Conformations in an Enzyme-Catalyzed Nucleophilic Bimolecular Reaction

S. Kashif Sadiq*,† and Peter V. Coveney*,‡

†Infection Biology Unit, Universitat Pompeu Fabra, Barcelona Biomedical Research Park (PRBB), C/Doctor Aiguader 88, 08003 Barcelona, Spain

‡Centre for Computational Science, Department of Chemistry, University College London, London WC1H 0AJ, United Kingdom

Supporting Information

ABSTRACT: Near attack conformations (NACs) are conformations extending from the ground state (GS) that lie on the transition path of a chemical reaction. Here, we develop a method for computing the thermodynamic contribution to catalysis due to NAC formation in bimolecular reactions, within the limit of a classical molecular dynamics force field. We make use of the Bürgi–Dunitz theory applied to large-scale unbiased all-atom ensemble molecular dynamics simulations. We apply this to HIV-1 protease peptide hydrolysis, known to achieve a rate enhancement of $\sim 10^{11}$ ($\Delta G^{\ddagger}_{cat} \sim 15$ kcal/mol) over the uncatalyzed bimolecular reaction ($\Delta G^{\ddagger}_{non} \sim 30$ kcal/mol). The ground state consists of a nucleophilic water molecule bound to an octapeptide substrate in the active site. We first observe multiple and reversible binding of a nucleophilic water molecule into the active site giving a free energy of binding of $\Delta G = -1$ kcal/mol to form the GS. The free energy barriers for catalyzed and uncatalyzed NAC formation are both equivalent: $\Delta G^{\ddagger}_{NAC} = 4.6$ kcal/mol, constituting ~30% and ~15% of the overall barriers, respectively. Therefore, not only does adoption of NACs only account for minor progress along the transition path in both catalyzed and uncatalyzed reactions, but there is no preferential formation of them in the catalyzed reaction. Analysis of the catalytic hydrogen bond network reveals interactions that stabilize the GS; however, subsequent NAC formation does not preferentially favor any of the possible hydrogen bond configurations. This supports the view that the catalytic power of HIV-1 protease is not due to NAC formation.

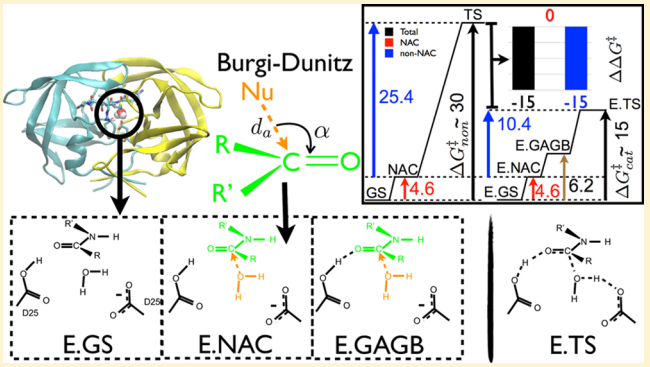

INTRODUCTION

The enormous rate enhancement afforded by enzymes (up to 10^{17} in some cases) has long been proposed to stem from tighter binding free energy of the transition state (TS), ΔG°_{TS}, as compared to the ground state (GS), ΔG°_{GS}, of a substrate undergoing chemical reaction.[1] From a thermodynamic perspective, this is entirely equivalent to the lowering of the activation free energy of the catalyzed reaction ($\Delta G^{\ddagger}_{cat}$) as compared to the uncatalyzed ($\Delta G^{\ddagger}_{non}$) reaction (Figure 1). This is because quantitative closure of the corresponding thermodynamic cycle in Figure 1 requires that $\Delta G^{\ddagger}_{cat} - \Delta G^{\ddagger}_{non} = \Delta G^{\circ}_{TS} - \Delta G^{\circ}_{TS}$.

However, this does not explain the mechanism for rate increase that can arise from a number of contributions, all of which are consistent with a generalized transition state theory (TST) framework.[2] This framework extends the original formulation of TST[3] to describe the rate constant of a chemical reaction as

$$k(T) = \gamma(T)(k_B T/h)(C^0)^{1-n}\exp[-\Delta G^{\ddagger}/RT] \quad (1)$$

where T is the temperature, R is the gas constant, C^0, is the standard state concentration of the reactant, n is the order of the reaction, $\Delta G^{\ddagger}$ is the standard-state free energy of activation, and $\gamma(T)$ is the generalized transmission coefficient.

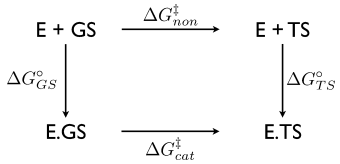

Figure 1. Thermodynamic cycle for binding of enzyme, E, to both the ground state, GS, and transition state, TS, of a substrate (ΔG°_{GS} and ΔG°_{TS}). The difference in binding free energy between the two states is equivalent to the difference between the uncatalyzed, ΔG°_{non}, and catalyzed, ΔG°_{cat}, activation free energy.

Rate enhancement via enzyme catalysis can then be afforded by lowering $\Delta G^{\ddagger}$ and/or raising $\gamma(T)$.

Alteration of the transmission coefficient $\gamma(T)$ is not overwhelmingly significant (affording rate enhancement up to 10^3), but it encompasses mechanisms such as quantum mechanical tunneling[4−6] and, still debated,[7] nonequilibrium intrinsic dynamical effects originating in the transfer of conformational changes in the enzyme into the chemical reaction coordinate.[8−13]

Received: October 1, 2014

   dx.doi.org/10.1021/ct5008845 | J. Chem. Theory Comput. XXXX, XXX, XXX−XXX

Enzyme and substrate flexibility can also lower or raise $\Delta G^{\ddagger}$ by altering the relative conformational free energy between the transition and reactant states.[14−16]

However, for many enzymes, the most significant factor underpinning enzyme catalysis is the lowering of the activation barrier ($\Delta G^{\ddagger}$) through preorganization of electrostatic interactions that favor formation of the TS.[17−23] An important byproduct of this is that the barrier for forming subsets of conformations in the GS ensemble can also be lowered, especially those that lie on the transition path nearer the TS.[24,25] Such conformations, termed near attack conformations (NACs), have been postulated before.[14,26−28] It was originally hypothesized that NAC conformations conferred a catalytic effect because they were attained readily in the enzyme but very rarely in water.[29,30] For example, in the unimolecular reaction catalyzed by chorismate mutase, the free energy of formation of a NAC has been shown to be reduced from 8.4 kcal/mol in water to 0.6 kcal/mol in the enzyme[29−31] thus providing evidence for relative thermodynamic stabilization of NACs over the GS, as compared with the uncatalyzed reaction. However, this has been challenged by studies reporting that electrostatic transition state stabilization accounts for the apparent NAC effect in chorismate mutase, specifically because there is very little change in the charge distribution going from GS to TS.[24,25] Other studies also report that NACs only moderately contribute to catalytic power.[32,33]

Computer simulation allows an extremely detailed analysis of such conformations at the molecular level, which is difficult to achieve via experiment. Despite the likely electrostatic molecular origin of NAC stabilization, calculating the thermodynamic difference between NAC formation in the catalyzed versus the uncatalyzed reaction is important because the reaction must still proceed through these conformations. Interestingly, such studies raise the prospect that whatever the molecular origins of barrier reduction are such effects may to an extent be accounted for by nonelectronic structural conformations and thus observable within the limit of a classical molecular dynamics force field. That is to say, variation of atomistic rather than electronic degrees of freedom might play at least some part in the catalysis.

Here, we develop a method for computing the thermodynamic contribution to catalysis due to NAC formation in bimolecular reactions within the limit of a classical molecular dynamics force field. Nucleophilic addition of a water molecule to carbonyl compounds to form a tetrahedral intermediate is a prime biological class of such reactions because it underpins proteolysis, a reaction ubiquitous in biology. Furthermore, analysis is made tractable by the Bürgi−Dunitz theory,[34−37] which describes the possible trajectory of the nucleophile. This permits definition of NACs in terms of a narrow nucleophile attack angle range and distance threshold with respect to the carbonyl system (Figure 2a).

In particular, we examine Bürgi−Dunitz type NAC formation in the peptide hydrolysis of a natural octapeptide substrate (p2-NC) by HIV-1 protease. This enzyme, together with its substrate complexes, has been crystallographically[38,39] and computationally[40−42] characterized at atomic resolution, making it a suitable choice to build on in developing our approach. The peptide corresponds to the C−N terminal junction between juxtaposed p2 and NC proteins in HIV-1 Gag and GagPol polyprotein chains, cleaved by the enzyme during maturation.

The accepted general acid/general base (GA/GB) reaction mechanism[43] is a two-step process that forms a metastable gem−diol intermediate. We focus on the first step, which is the

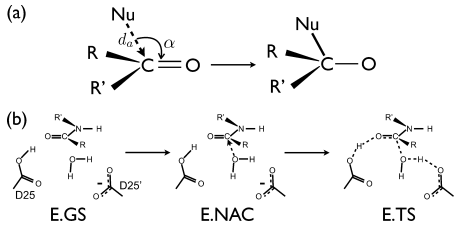

Figure 2. (a) Bürgi−Dunitz trajectory for nucleophilic addition to a carbonyl compound to form a tetrahedral intermediate. Successful attack by the nucleophile (Nu) requires approach in a narrow angle range of $\alpha = 105 \pm 5°$ and attack distance $d_a \leq 3.2$ Å. (b) First stages of a general acid/general base mechanism for proteolytic cleavage by the catalytic monoprotonated aspartyl dyad (D25/D25′) of HIV-1 protease involving an enzyme bound ground state (E.GS) changing into a NAC (E.NAC) when the nucleophilic water oxygen fulfils the Bürgi−Dunitz criteria and on into the tetrahedral transition state (E.TS).

one relevant to NAC formation and which presents the largest single-step barrier.[44] The catalytic aspartyl dyad (D25/D25′) has a monoprotonated D25 state[45−47] in an asymmetric conformation,[48] which promotes a nucleophilic water attack via hydrogen bonding between the protonated D25 residue and carbonyl oxygen adjacent to the peptide bond (Figure 2b and Figure 3a). In crystal structures, a non-nucleophilic water

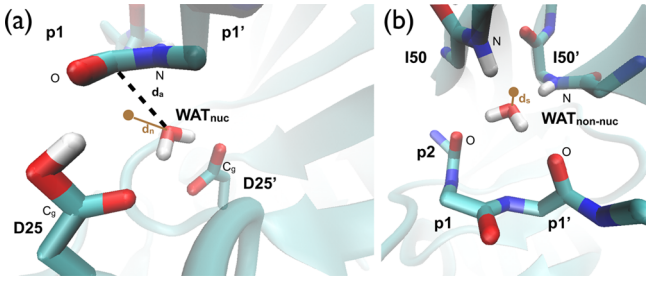

Figure 3. (a) Geometry of the catalytic site in HIV-1 protease complexed with both a substrate and a nucleophilic water molecule (WAT_{nuc}). The nearest water attack distance to the peptide bond carbon (d_a) and the distance of the nearest water (d_n) to the catalytic center (o_{cat}:brown dot), the geometric center between the four atoms, p1:C, p1′:N, D25:CG, and D25′:CG, are represented. (b) Geometry of the non-nucleophilic water ($WAT_{non-nuc}$) binding site within the flap−substrate interface. The nearest distance of this structural water molecule (d_s) to the geometric center (o_{struct}:brown dot) of the tetrahedral group, comprising the backbone nitrogen atoms of I50/I50′ residues and carbonyl oxygens of the p2 and p1′ residues of the substrate, are represented.

molecule is also found tetrahedrally bound at the interface between the β-hairpin flaps and the substrate (Figure 3b), locking the enzyme−substrate complex in a catalytically viable conformation.[49]

Experimentally,[50] the reaction rate of this system yields $k_{cat} \sim 40\ s^{-1}$ or $\Delta G^{\ddagger} \sim 15$ kcal/mol (assuming $\gamma = 1$). By comparison, the half-life of uncatalyzed peptide hydrolysis in water is ~500 years,[51] resulting in $\Delta G^{\ddagger}_{non} \sim 30$ kcal/mol.

Although the enzyme-catalyzed reaction follows a different mechanism from that in solution, NAC formation in free reactant and the enzyme-bound case is equivalent as long as the Bürgi−Dunitz criteria are fulfilled. In a bimolecular reaction, the ground state GS is defined in terms of conformations corresponding to bound states of the two reactants, in this case the p2-NC octapeptide and a single nucleophilic water molecule.

dx.doi.org/10.1021/ct5008845 | J. Chem. Theory Comput. XXXX, XXX, XXX−XXX

The free energy for the formation of a NAC is quantified by calculating the mole fraction of NAC relative to GS during an ensemble of 100 ns × 100 ns unbiased all-atom explicit solvent molecular dynamics simulations of HIV-1 protease complexed with p2-NC octapeptide. We compare this to the free energy of forming a NAC in the uncatalyzed reaction, calculated from 10 × 1 μs control simulations of the p2-NC octapeptide in explicit solvent, allowing us to calculate the contribution of NACs in the catalytic process. We are also able to reconstruct the thermodynamics of nucleophilic water entry/exit from the catalytic site and to construct a complete thermodynamic network of catalytic hydrogen bonding for when a water molecule is in the catalytic site.

METHODS

Initial System Preparation. Initial structures were prepared for the p2-NC (ATIM-MQRG) octapeptide substrate in apo-ligand form and bound to HIV-1 protease complex. Atomic coordinates for a wildtype dimeric HIV-1 protease complex and the apo-substrate were extracted from the 1KJ7 crystal structure in the Protein Data Bank.[52] The inactive catalytic dyad D25N was converted into catalytically active D25 form with a monoprotonated state.[47,53] Crystallographic water molecules in 1KJ7 were preserved. An additional water molecule was inserted between the lytic peptide bond and the catalytic dyad as is expected in the general acid/general base (GA/GB) cleavage mechanism.[54] The standard AMBER force field (ff03)[55] was used to describe all parameters. Each system was solvated using atomistic TIP3P water[56] and then electrically neutralized with an ionic concentration of 0.15 M NaCl, resulting in fully atomistic and explicit solvent systems of approximately 40,000 atoms and 14,000 atoms, respectively.

Equilibration and Simulation Protocol. Conjugate-gradient minimization was performed. The SHAKE algorithm[57] was employed on all atoms covalently bonded to a hydrogen atom for stages of each simulation whose time step was greater than 1 fs. The long-range Coulomb interaction was handled using a GPU implementation[58] of the particle mesh Ewald summation method (PME).[59] A nonbonded cutoff distance of 9 Å was used with a switching distance of 7.5 Å. During equilibration, the position of all heavy protein atoms (including the catalytic water oxygen atom in the complex) was restrained by a 1 kcal/mol/Å^2 spring constant, and the system evolved for 1 ns at 300 K. For the complex system, the restraining constant was set to zero for all atoms except the C_γ atoms of the catalytic dyad, the lytic bond atoms, and the catalytic water oxygen to preserve the geometry of the cleavage region, and the system evolved for a further 1 ns. The restraining constant was then set to 0.1 kcal/mol/Å^2 for the catalytic water oxygen and set to zero for all other atoms, and the system evolved for a further 10 ns. An integration time step of 2 fs was used. For the apo-ligand system, restraints were set to 0.5 kcal/mol/Å^2 for all heavy protein atoms, and the system evolved for 10 ns with a time step of 4 fs. The temperature was maintained at 300 K using a Langevin thermostat with a low damping constant of 0.1/ps, and the pressure was maintained at 1 atm for both systems. The sytems were then equilibrated for 10 ns of unrestrained simulation in the canonical ensemble (NVT) with an integration time step of 4 fs. The final coordinates were used as input for production simulations, which were carried out using ACEMD[60] in the NVT ensemble with a 4 fs time step. Coordinate snapshots from production simulations were generated every 100 and 10 ps for complex and apo-ligand systems, respectively. The EMERALD GPU cluster was used to generate apo-ligand trajectories; complexed trajectories were generated as part of a previous effort[61] on the GPUGRID.net infrastructure.[62] Experimental accuracy of our molecular simulation protocol for the HIV-1 protease has been previously validated using NMR S^2 order parameters.[63] Two force field variation studies for the apo-ligand system were also performed, each with an identical protocol and production simulation time (10 × 1 μ s), but using the modified AMBER force field (ff99SBildn)[64] while retaining the TIP3P water model and using the TIP4P water model[56] while retaining the standard Amber force field (ff03).

Analysis. *Nearest Water Analysis.* The geometric center between the four atoms, p1:C, p1′:N, D25:CG, and D25′:CG, was chosen as the center of the catalytic site (o_{cat}). The nearest water distance (d_n) was defined as the distance of the oxygen atom WAT:O of the nearest water molecule from this origin and from the center of p1:C−p1′:N for the enzyme-bound and apo-substrate systems respectively (Figure 3 and Table 1).

Table 1. Definitions of Nearest Water Bürgi−Dunitz Attack Distance (d_a), Angle (α), and Distance of Nearest Water (d_n) to Catalytic Center (o_{cat}); d_n(apolig), Corresponding to Distance from the Center (o_{apolig}) of the p2-NC Apo-Substrate System, and d_s, Corresponding to Distance of Non-Nucleophilic Water Molecule from Its Tetrahedral Geometric Center (o_{struct})

center name	atoms defining geometric center
o_{cat}	p1:C, p1′:N, D25:CG, D25′:CG
o_{struct}	p2:C, p1′:C, I50:N, I50′:N
o_{apolig}	p1:C, p1′:N
metric	**definition**
α	WAT:O-p1:C-p1:O
d_a	WAT:O-p1:C
d_n	WAT:O-o_{cat}
d_n(apolig)	WAT:O-o_{apolig}
d_s	WAT:O-o_{struct}

The near attack distance (d_a) was defined as the distance between the carbon atom of the lytic peptide bond (p1:C) and the oxygen atom of the nearest water molecule (WAT:O).

Potential of Mean Force and Free Energy Calculations. Potentials of mean force were calculated by binning ensemble data into microstates corresponding to the reaction coordinate space and then calculating the mole fraction (ρ) of each microstate using $\Delta G = -k_B T ln(\rho)$. Free energy differences (ΔG) between various states were calculated similarly from the ratios of the corresponding mole fractions according to $\Delta G = -k_B T ln(\rho_2/\rho_1)$, where ρ_1 and ρ_2 are mole fractions of any given states 1 and 2, respectively. To calculate errors, the entire simulation ensemble for both systems was partitioned into five subsets each; mole fractions were calculated independently in each subset and averaged to yield means and standard deviations. States A−D were defined by assigning geometrical boundaries around the corresponding minima within the d_n−d_a−α space (Table 2); the NAC state was defined according to the Bürgi−Dunitz criteria of $d_a \leq 3.2$ Å and $100° \leq \alpha \leq 110°$ for nucleophilic attack. Sensitivity of the free energy difference for NAC formation upon varying the Bürgi−Dunitz metrics was assessed.

Hydrogen Bond Network Analysis. We constructed a 16-state hydrogen bond network corresponding to the cooperative permutations of four independent hydrogen bonds (Figure 7).

dx.doi.org/10.1021/ct5008845 | J. Chem. Theory Comput. XXXX, XXX, XXX−XXX

Table 2. Boundary Definitions of Conformations A–D and NAC in Terms of d_n, d_a, and α Thresholds

conformation	definition
A	2 Å ≤ d_n ≤ 4 Å, 3.5 Å ≤ d_a ≤ 4.5 Å, 140° ≤ α ≤ 160°
B	3.5 Å ≤ d_n ≤ 4.5 Å, 5 Å ≤ d_a ≤ 6 Å, 70° ≤ α ≤ 100°
C	5 Å ≤ d_n ≤ 6 Å, 3.5 Å ≤ d_a ≤ 4.5 Å, 10° ≤ α ≤ 30°
D	5 Å ≤ d_n ≤ 6 Å, 3.5 Å ≤ d_a ≤ 4.5 Å, 90° ≤ α ≤ 120°
NAC	d_n ≤ 4.6 Å, d_a ≤ 3.2 Å, 100° ≤ α ≤ 110°

The threshold for a hydrogen bond was a donor–acceptor distance ≤3.5 Å and donor–hydrogen–acceptor distance of ≥150°. The time evolution of each hydrogen bond was calculated across all trajectories, taking care to integrate the possible degenerate configurations pertaining to each independent bond that arise from structural symmetries imposed by molecular rotation (Table 3), and from this the frequency of each state of the hydrogen bond network was analyzed for conformations A–D and NAC.

Table 3. Possible Donor–Hydrogen–Acceptor Configurations and Corresponding Definitions for Hydrogen Bonds (hb1–hb4) in Conformational Geometry of Catalysis

H bond	configuration	donor–hydrogen–acceptor definition
hb_1	HB1	D25:O2 D25:H p1:O
hb_2	HB21	D25:O2 D25:H D25′:O1
	HB22	D25:O2 D25:H D25′:O2
hb_3	HB311	WAT:O WAT:H1 D25′:O1
	HB312	WAT:O WAT:H2 D25′:O1
	HB321	WAT:O WAT:H1 D25′:O2
	HB322	WAT:O WAT:H2 D25′:O2
hb_4	HB411	WAT:O WAT:H1 D25:O1
	HB412	WAT:O WAT:H2 D25:O1

RESULTS

Reversible Nucleophilic Water Binding and Near Attack Conformations. Enzyme-complexed simulations were initiated with manual placement of a water molecule in the catalytic site. However, nucleophilic water dissociation and subsequent association were observed in many trajectories (Figure S1 and Movie M1 (zip file), Supporting Information). We account for nucleophilic water binding and dissociation by calculating the distance of the nearest water molecule (d_n) to the origin of the catalytic site (Methods). The normalized frequency distribution (ρ (d_n)) of the nearest water distance exhibits two well-defined maxima at 3.4 and 5.8 Å, respectively (Figure 4a). The first peak is the dominant one, corresponding to a nucleophilic water molecule in the catalytic site. The second maximum is expected due to the existence of the non-nucleophilic water molecule that contributes to binding the ligand to the enzyme. This "structural" water molecule remains within 2 Å of its central position for virtually the entire (99.84%) simulation ensemble (Figure 4b), exhibiting a single peak at a distance of 0.5 Å. Thus, when the nucleophilic water molecule departs the catalytic site, the nearest water predominantly switches to being the non-nucleophilic water molecule. This switching is sharp (occurring at d_n ≥4.6 Å), which defines a natural reaction coordinate partition between the bound and unbound domain of the nucleophilic water molecule in terms of d_n. The free energy of nucleophilic water binding (ΔG_{nwb}) is calculated in terms of the mole fraction of bound and unbound states in this reaction coordinate space, yielding $\Delta G_{nwb} = -1.0 \pm 0.3$ kcal/mol.

We calculated the Bürgi–Dunitz nucleophilic attack distance d_a and attack angle, α. Unlike d_n, d_a does not exhibit sharp transitions (Figure S2, Supporting Information), but nonetheless it exhibits a noticeable bimodal distribution (Figure 4c), again representative of the occurrence of a lytic water molecule in the catalytic site (minor peak) as well the distance of the structural water molecule from the peptide carbon (major peak). The latter is the major peak because of the additional water molecules that are proximal to the peptide carbon without being near to the center of the catalytic site.

A more detailed inspection of the nearest water position can be made by plotting the distribution of points in a 3d space consisting of d_n, d_a, and α (Figure 5a). This reveals the existence of four distinct structural clusters (A–D) in the data set. Potential of mean force (PMF) calculations (Figure 5b) in 2D projections of this space for (i) d_a-α and (ii) d_n–α show minima at 5, 6, 4, and 3 kcal/mol corresponding to clusters A–D, respectively. Structural correspondence of these minima is shown in Figure 5c. Minima A and B correspond to a nucleophilic water molecule in the catalytic site with oxygen oriented toward and away from the peptide bond, respectively. Minimum C corresponds to when the non-nucleophilic water molecule is nearest to the catalytic site. Minimum D corresponds to a small population of events when a nucleophilic water molecule is at the edge of the catalytic site. The bound and unbound peaks observed in Figure 5 thus each constitute two conformations of nearest water molecules.

None of the four conformational minima defined above fulfill the Bürgi–Dunitz criteria of d_a ≤3.2 Å and 100° ≤ α ≤ 110° for

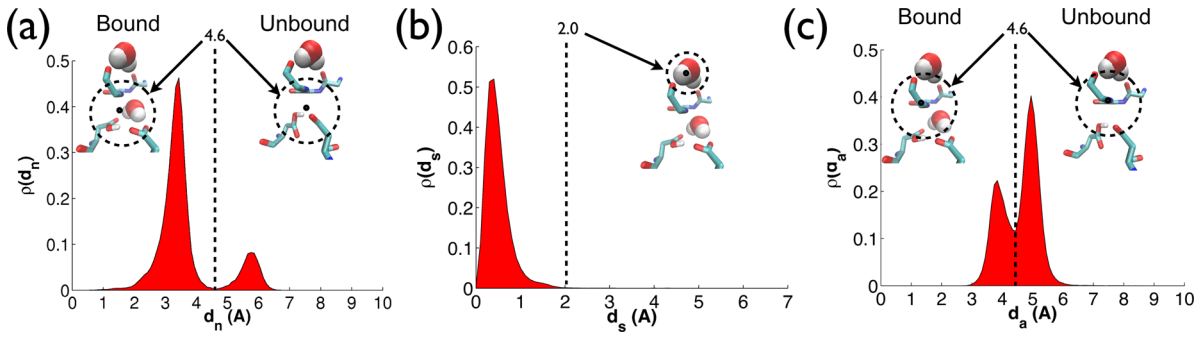

Figure 4. Normalized frequency distributions (ρ) of (a) distance of the nearest water (d_n) to the catalytic center (o_{cat}), (b) distance of the nearest structural water molecule (d_s) to the structural water center (o_{struct}), and (c) nearest water attack distance (d_a) to the peptide bond carbon.

dx.doi.org/10.1021/ct5008845 | J. Chem. Theory Comput. XXXX, XXX, XXX–XXX

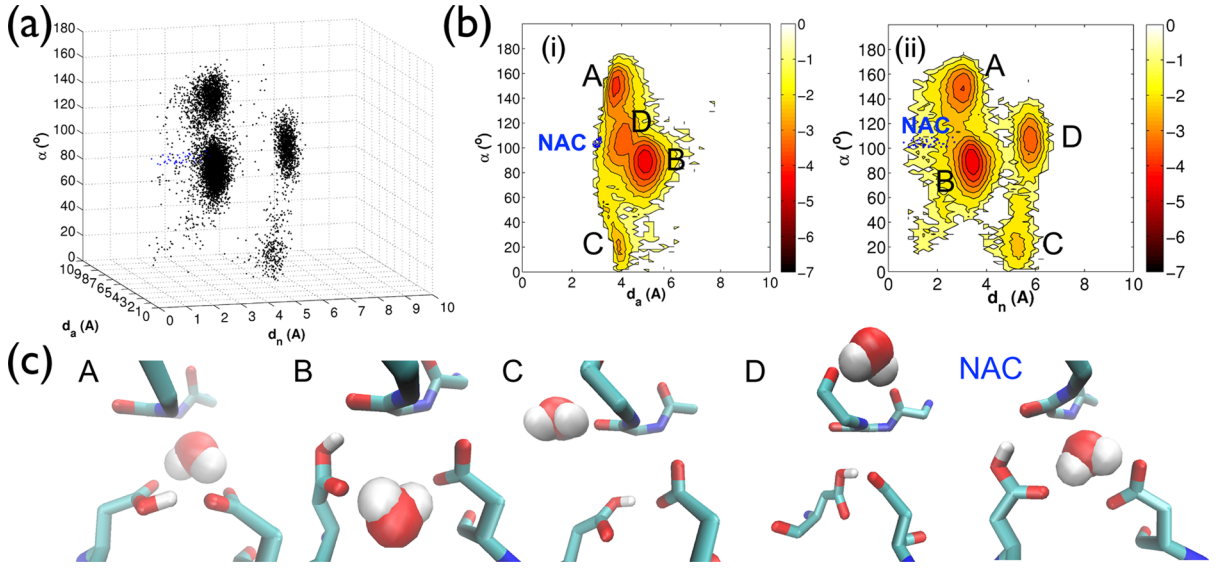

Figure 5. (a) 3D plot of nearest water molecule position in terms of d_n as well as the Bürgi–Dunitz distance (d_a) and angle (α) metrics. Four distinct conformational populations are visible (A–D); NACs are plotted in blue. (b) Potential of mean force in reduced 2D plots of (i) d_a–α and (ii) d_n–α reaction coordinates. NACs are fringe conformations occupying no minima (plotted in blue). (c) Structural representation of the four minima (A–D) and a NAC.

nucleophilic attack. Only 0.042% of water molecule conformations fulfilled these criteria, 0.038% being within the catalytic site ($d_n \leq 4.6$ Å) and 0.004% outside it ($d_n > 4.6$ Å). As is observable in Figure 5b, these events do not constitute a minimum in the data set (NAC: blue points). Visual inspection of these states confirms that the nucleophilic water molecule is within the catalytic site with oxygen oriented in the correct direction favorable for chemical reaction (Figure 5c). The events outside the catalytic site are all due to rare occurrences of the nearest water approaching the active site and are discarded. Attainment of a NAC is thus a rare event with a free energy difference relative to the ground state of $\Delta G^{\ddagger}_{NAC}$ = 4.6 ± 0.2 kcal/mol. Varying the threshold of d_n that constitutes a bound state is stable right up to distances approaching the Bürgi–Dunitz threshold (Figure 6a). Sensitivity of the free energy difference for NAC formation upon varying the Bürgi–Dunitz metrics was also assessed (Figure S3, Supporting Information). The free energy is insensitive to variation of the angle and only moderately sensitive to distance.

We analyzed control simulations of a p2-NC octapeptide apo-substrate in explicit solvent, determining the nearest water distance from the lytic peptide bond as well as the Bürgi–Dunitz metrics (Methods). In this case, 0.0256% of water molecules fulfilled the original Bürgi–Dunitz criteria; however, unlike for the enzyme complex, defining a GS bound conformation is not trivial. The nearest water distance (d_n) was calculated with respect to the middle of the lytic peptide bond. However, there was no sharp cut off in the probability density between bound and unbound water molecules, and thus, $\Delta G^{\ddagger}_{NAC}$ steadily decreases with decreasing d_n from an initial maximum plateau that corresponds to the maximum ligand–water distance in solvent (Figure 6b). Nonetheless, by assuming the bound state as this maximum, we are able to calculate a theoretical upper limit of NAC free energy relative to the GS of $\Delta G^{\ddagger}_{NAC} \leq 4.6 \pm 0.1$ kcal/mol.

In order to check the force field sensitivity of our results, we reproduced the control simulations using an alternative force field (ff99SBildn) and using a different water model (TIP4P)

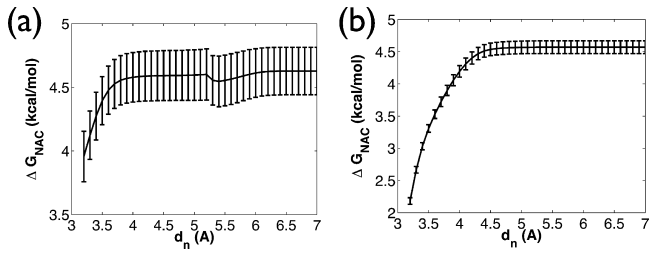

Figure 6. (a) Free energy of NAC formation ($\Delta G^{\ddagger}_{NAC}$) for the HIV-1 protease p2-NC substrate water complex when varying the threshold of d_n that constitutes a bound state. $\Delta G^{\ddagger}_{NAC}$ exhibits a steady plateau at 4.6 ± 0.2 kcal/mol, only decreasing when d_n approaches the Bürgi–Dunitz threshold of 3.2 Å. The slight dip in the plateau corresponds to the clear partition between bound and unbound states exhibited in the normalized probability density (ρ (d_n)) of nearest water molecule distance (Figure 4a). (b) Free energy of NAC formation ($\Delta G^{\ddagger}_{NAC}$) for the p2-NC apo-ligand when varying the threshold of d_n that constitutes a bound state. $\Delta G^{\ddagger}_{NAC}$ exhibits a steady plateau also at 4.6 ± 0.1 kcal/mol until $d_n \sim 4.4$ Å, after which it decreases more rapidly than the enzyme-bound system as d_n approaches the Bürgi–Dunitz threshold of 3.2 Å. Although there is no clear partition in the normalized probability density (ρ (d_n)) of nearest water molecule distance, $\Delta G^{\ddagger}_{NAC}$ is stable around the value of d_n = 4.6 Å that corresponds to a bound state in the enzyme complexed state. The plateau also represents the theoretical upper limit of NAC free energy relative to the GS.

with explicit polarizability. The nearest water distance profiles for these alternatives varied only slightly from the ff03-TIP3P distribution (Figure S4, Supporting Information), and using a similar approach, the theoretical upper limit of NAC free energy relative to the GS was calculated as $\Delta G^{\ddagger}_{NAC} \leq 3.7 \pm 0.1$ kcal/mol and $\Delta G^{\ddagger}_{NAC} \leq 3.6 \pm 0.1$ kcal/mol, respectively. These represent variations of 0.9 and 1.0 kcal/mol respectively, which are only slightly larger than thermal noise. Therefore, to a good approximation, the absolute contribution to NAC formation in both the catalyzed and uncatalyzed reactions can be treated as almost equivalent.

dx.doi.org/10.1021/ct5008845 | J. Chem. Theory Comput. XXXX, XXX, XXX–XXX

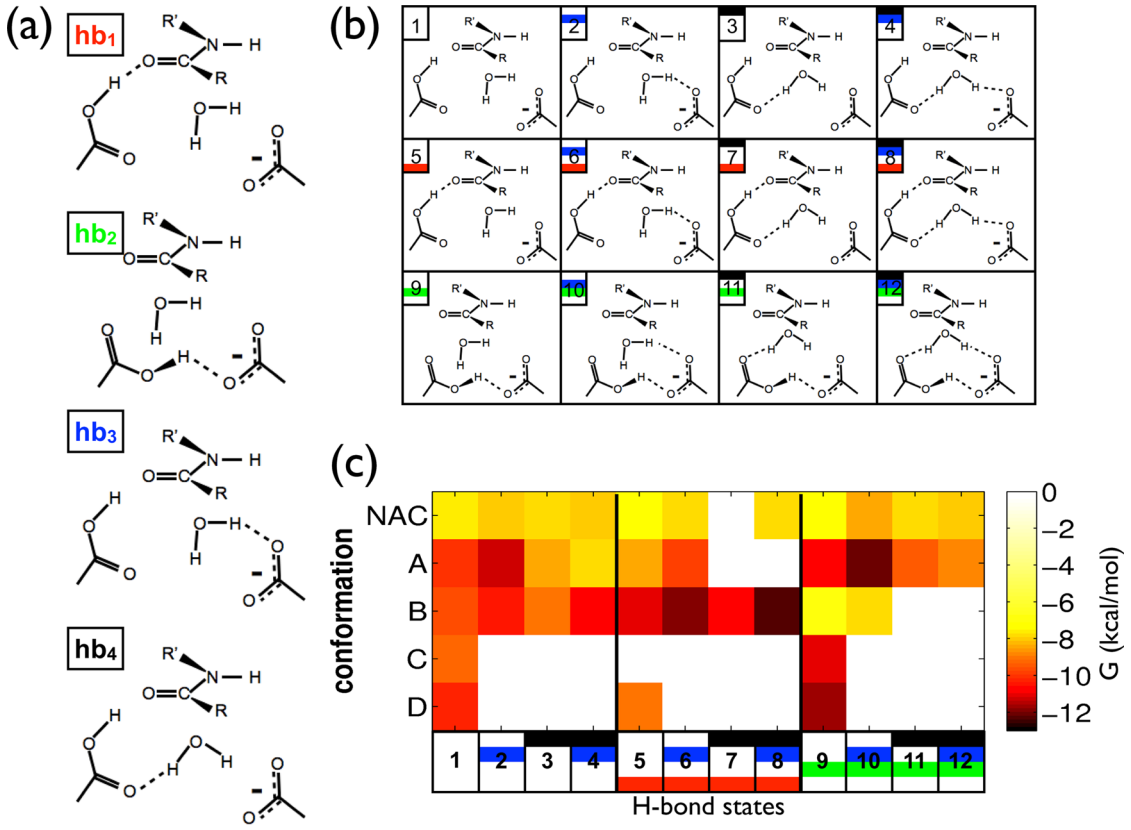

Figure 7. (a) Four independent hydrogen bonds (hb1−hb4) involving the nucleophilic water molecule, catalytic D25/D25′ dyad, and carbonyl oxygen. (b) Possible states (1−12) of the hydrogen bond network that arise from hydrogen bonds hb1−hb4. The existence of each hydrogen bond in a particular state is color coded with hb1 (red), hb2 (green), hb3 (blue), and hb4 (black). (c) Thermodynamics of each state of the hydrogen bond network for each of the nearest water conformations A−D as well as NAC.

Thermodynamics of Catalytic Hydrogen Bond Network. In general, the number of distinct hydrogen bond configurations possible involving the peptide bond, D25/D25′ dyad, and a nucleophilic water molecule is not limited to those required for catalysis under the GA/GB mechanism. Therefore, in order to understand the role of hydrogen bonding in affecting catalysis, we constructed a network from the possible hydrogen bonds that could exist when a nucleophilic water molecule is in the catalytic site. Four distinct hydrogen bonds (hb1−hb4) can be formed between the catalytic Asp dyad, carbonyl oxygen of the peptide bond, and nucleophilic water molecule (Figure 7a); several consist of degeneracies due to the possible molecular rotations (Table 3). Two of these, hb1 and hb2, involve only D25, D25′, and/or the carbonyl oxygen of the peptide bond. The other two, hb3 and hb4, are formed between the catalytic water molecule and oxygen atoms of D25′ and D25, respectively. Permutations corresponding to the possibility of simultaneously existing hydrogen bonds gives rise to a network of 16 states. However, hb1 and hb2 are found not to coexist (Figure S5, Supporting Information) due to the stoichiometry of the catalytic site. This reduces the network to effectively 12 states (Figure 7b). Under such a scheme, the hydrogen bond configuration consistent with the GA/GB mechanism is defined by state 6. We analyzed the thermodynamics of each state of the hydrogen bond network across all conformations A−D that corresponded to various stages of nucleophilic water entry as well as for NACs (Figure 7c).

Conformations C and D correspond to situations when no water molecule is in the catalytic site. Therefore, the only states possible are 1 (no hydrogen bonds), 5 (hb1 only), and 9 (hb2 only). For both conformations, state 9 (only hb2) is favored thermodynamically (C, −4.2 kcal/mol; D, −4.8 kcal/mol), followed by state 1 (C, −2.3 kcal/mol; D, −3.4 kcal/mol). State 5 (only hb1) is exhibited in D (−2.2 kcal/mol) but not in C. This is because conformation C corresponds to a water molecule interacting with the carbonyl oxygen of the peptide bond, preventing interaction of the latter with the hydroxyl moiety of D25.

Entry of a water molecule into the catalytic site permits formation of hb3 and hb4. For conformation B, the population of any state containing hb2 (states 9−12) is severely reduced (G = −1.2 kcal/mol). There is a strong thermodynamic shift toward hb1-containing states (states 5−8) with G = −5.8 kcal/mol; these become the dominant thermodynamic states, followed by states 1−4 (containing neither hb1 nor hb2) with G = −4.3 kcal/mol. Within hb1-containing states, state 8 is dominant (G = −5.5 kcal/mol), followed closely by state 6 (G = −5.0 kcal/mol).

Adoption of conformation A results in another thermodynamic shift back toward hb2-containing states (G = −5.4 kcal/mol), all with significant population and with state 10 exhibiting dominance (G = −5.3 kcal/mol). There is a shift away from hb1-containing states (G = −3.2 kcal/mol), within which a redistribution of states strongly in favor of state 6 occurs (G = −3.1 kcal/mol) with there being no longer any population of state 7 or 8. The population of states containing neither hb1 nor hb2 stays approximately the same (G = −4.6 kcal/mol), although there is a slight redistribution toward state 2 (G = −4.5 kcal/mol).

dx.doi.org/10.1021/ct5008845 | J. Chem. Theory Comput. XXXX, XXX, XXX−XXX

Furthermore, no thermodynamic preference is exhibited for the formation of a NAC in terms of the hydrogen bond network, while all NACs are, as expected, sparsely populated (> −1.7 kcal/mol). Therefore, fulfilment of the Bürgi−Dunitz conditions alone is not concomitant with a restriction in the hydrogen bond state distribution toward state 6, necessary for initiation of the GA/GB mechanism for catalysis. We interpret this as arising from the rotational flexibility of the nucleophilic water molecule as well as the Asp dyad being sufficiently large to prevent stable formation of any one set of hydrogen bond states when within the Bürgi−Dunitz criteria.

Finally, only 0.003% of all conformations simultaneously fulfilled both the Bürgi−Dunitz NAC criteria and the hydrogen bonding conditions (state 6) required by the GA/GB mechanism. This results in a hydrogen bond contribution to $\Delta G^{\ddagger}_{cat}$ relative to NAC formation of $\Delta G^{\ddagger}_{hb}$ = 1.6 ± 1.2 kcal/mol, with the overall barrier to form this state being $\Delta G^{\ddagger}_{gagb}$ = 6.2 ± 1.4 kcal/mol from the GS.

DISCUSSION AND CONCLUSIONS

For nucleophilic bimolecular reactions, we have developed a computational approach for calculating the degree to which the catalytic effects of an enzyme are manifested within thermodynamic changes in the reaction's structural degrees of freedom, that is, as a result of preferential formation of atomistic conformations, termed near attack conformations (NACs), that lie on the reaction path.

We have applied the method to the bimolecular reaction catalyzed by HIV-1 protease, using unbiased all-atom ensemble explicit solvent molecular dynamics simulations of the protease complexed to the p2-NC octapeptide. In order to understand whether any catalytic effect exists as a result of preferential NAC formation, it is necessary to compare against the thermodynamics of NAC formation in the free solution reaction. We therefore compared our results with reference simulations of the p2-NC apo-substrate in solution.

Comprising conformations for which a water molecule is within the distance−angle criteria that permit nucleophilic attack of the peptide bond, according to Bürgi−Dunitz theory, we calculated a free energy for NAC formation of only $\Delta G^{\ddagger}_{NAC}$= 4.6 ± 0.1 kcal/mol in the free solution reaction. This accounts for only 15.3% of the overall barrier in the uncatalyzed system (~30 kcal/mol) and represents the maximum possible contribution to catalysis from NAC formation, leaving a 25.4 kcal/mol barrier to be overcome by electronic contributions (Figure 8).

For the enzyme-catalyzed system, the overall barrier to form the first transition state is ~15 kcal/mol (Figure 8). In order for the catalytic effect to be manifested structurally, the NAC free energy of formation needs to be significantly reduced in the catalyzed as compared to the uncatalyzed case. However, we calculated a free energy for NAC formation of also $\Delta G^{\ddagger}_{NAC}$= 4.6 ± 0.2 kcal/mol in the enzyme catalyzed case, therefore, equivalent to the free solution. NAC formation thus represents only ~30% of the overall catalyzed reaction barrier ($\Delta G^{\ddagger}_{cat}$ ~ 15 kcal/mol) and thus only a minor fraction both in the catalyzed and uncatalyzed reactions. More importantly, no catalytic effect is observed as a result of thermodynamically favored NAC formation in the enzyme-bound case as compared to the free peptide, consistent with recent density functional theory (DFT)-based approaches.[65] Electronic contributions thus account for ~15 kcal/mol worth of catalytic power.

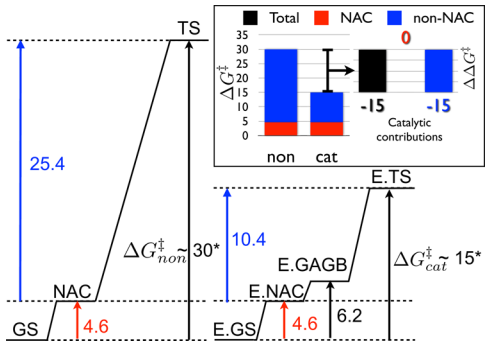

Figure 8. Schematic activation energy diagrams for the uncatalyzed and catalyzed reactions respectively, showing the contribution of NACs and GA/GB hydrogen bond state (GAGB) across the transition state pathway (main diagram). The overall activation barriers $\Delta G^{\ddagger}_{non}$ and $\Delta G^{\ddagger}_{cat}$ are calculated from the experiment.[50,51] Inset shows how the total energy barrier decreases due to catalysis (black) and is decomposed in terms of NAC (red) and non-NAC (blue) contributions. All values are in kcal/mol.

Recently, it was suggested that the rate-limiting step in HIV-1 protease catalysis was the emergence of a catalytically preorganized active site in the unliganded enzyme, where the asymmetric dyad configuration, required for the GA/GB mechanism, was correlated to asymmetric β-hairpin flap isomerizations and higher mobility of the left flap.[48] On the one hand, this qualitatively implicates dynamic coupling. Such an effect may prove to play a significant role if it can be shown that conformational fluctuations in the enzyme directly affect electronic degrees of freedom along the reaction path.

On the other hand, it could also be interpreted as a thermodynamic effect, the verification of which awaits equilibrium quantification of relative isomer popluations both in the unliganded and liganded case. Nonetheless, this contribution is likely to be small as the native asymmetric isomerization should be the thermodynamically favorable one. Our simulations, performed in the native asymmetric closed flap state, concur that the left flap exhibits higher mobility through uncurling, while virtually no isomer exchange is exhibited over the 10 μs ensemble (Figure 9). Longer simulations will thus be needed to probe this effect.

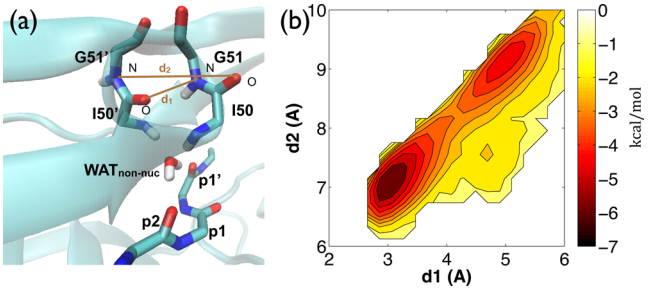

Figure 9. Potential of mean force calculations (kcal/mol) of the Gly51:N-Ile50′:O and Ile50:O-Gly51′:N distances, termed $d1$ and $d2$, respectively, calculated from the entire simulation ensemble. The major well corresponds to an isomer characterized by Gly51:N-Ile50′:O hydrogen bonding (d_1 <3.5 Å), and the minor well corresponds to a ~2 Å uncurling of only the left flap. There is no exchange to the alternate asymmetric isomer characterized by Ile50:O-Gly51′:N hydrogen bonding (d_2 <3.5 Å) and only trace instances of exchange to a left-symmetric isomer (d_1 >4.5 Å and d_2 <7.5 Å). Longer simulations are thus needed to establish the equilibrium effect of isomer exchange on the preorganization within the catalytic site.

dx.doi.org/10.1021/ct5008845 | J. Chem. Theory Comput. XXXX, XXX, XXX−XXX

The major candidate for the origin of catalytic power in HIV-1 protease is electrostatic preorganization in the active site. The GA/GB hydrogen bond conformation represents an extremely favorable dipole preorientation for the transition state, confirmed experimentally.[66] Our study supports the view that the effects of this electrostatic preorganization are manifested only near the transition state and reduce the barrier solely along the electronic degrees of freedom. Otherwise, the force field used here, which accounts for the structural component of such effects, would have led to significant differences in NAC populations in the catalyzed and uncatalyzed systems. Our analysis of the hydrogen bond network also reveals non-GA/GB interactions as well as no particular bias during NAC exhibition (Figure 7), which amounts to only a further penalty of $\Delta G^{\ddagger}_{hb}(enz) = 1.6 \pm 1.2$ kcal/mol to form the GA/GB conformation in the enzyme.

Finally, the method we have developed can be applied to any system involving second order nucleophilic interactions, provided enough statistics are obtained for NAC observation and a meaningful definition for what constitutes the GS is chosen. Reactions involving water are simplest to achieve due to it constituting the bulk solvent. Furthermore, the existence of a proximal and stable non-nucleophilic water molecule aids in the sharpness of bound−unbound partitioning, observed here. Nonetheless, top-end high throughput molecular simulation architectures have reached the millisecond time scale,[67] which should soon allow the method to be applied to reactions involving multiple numbers and species of larger substrates.

■ ASSOCIATED CONTENT

Supporting Information

Movie of catalytic water disassociation/reassociation, time evolution graphs, free energy sensitivity plot, and force field variation plot. This material is available free of charge via the Internet at http://pubs.acs.org.

■ AUTHOR INFORMATION

Corresponding Authors

*E-mail: kashif.sadiq@upf.edu, syedkashifsadiq@gmail.com (S.K.S).

*E-mail: p.v.coveney@ucl.ac.uk (P.V.C.).

Notes

The authors declare no competing financial interest.

■ ACKNOWLEDGMENTS

We are grateful to Prof. Adrian Mulholland for reading the manuscript and for helpful discussions. The authors thank Dr. Gianni De Fabritiis for previous use of the GPUGRID.net infrastructure. The work presented here made use of the EMERALD HPC facility provided by the e-Infrastructure South Centre for Innovation (EPSRC grant refs EP/K000144/1, EP/K000136/1). P.V.C. thanks the EU FP7 CHAIN (HEALTH-2007-2.3.2-7) and the UCL CLMS Network. S.K.S. acknowledges support from amfAR Mathilde Krim Fellowship in Basic Biomedical Research number 108680.

■ REFERENCES

(1) Pauling, L. *Chem. Eng. News.* **1946**, *24*, 1375−1377.
(2) Garcia-Viloca, M.; Gao, J.; Karplus, M.; Truhlar, D. *Science* **2004**, *303*, 186−195.
(3) Eyring, H.; Stearn, A. *Chem. Rev.* **1939**, *24*, 253−270.
(4) Cui.; et al. *J. Am. Chem. Soc.* **2002**, *124*, 3093−3124.
(5) Masgrau, L.; Roujeinikova, A.; Johannissen, L.; Hothi, P.; Basran, J.; Ranaghan, K.; Mulholland, A.; Sutcliffe, M.; Scrutton, N.; Leys, D. *Science* **2006**, *312*, 237−241.
(6) Gao, J.; Truhlar, D. *Annu. Rev. Phys. Chem.* **2002**, *53*, 467−505.
(7) Pisliakov, A.; Cao, J.; Kamerlin, S.; Warshel, A. *Proc. Natl. Acad. Sci. U.S.A.* **2009**, *106*, 17359−17364.
(8) Careri, G.; Fasella, P.; Gratton, E.; Jencks, W. *Crit. Rev. Biochem. Mol. Biol.* **1975**, *3*, 141−164.
(9) Welch, G.; Somogyi, B.; Damjanovich, S. *Prog. Biophys. Mol. Biol.* **1982**, *39*, 109.
(10) Olsson, M.; Parson, W.; Warshel, A. *Chem. Rev.* **2006**, *106*, 1737−1756.
(11) Eisenmesser, E.; Millet, O.; Labeikovsky, W.; Korzhnev, D.; Wolf-Watz, M.; Bosco, D.; Skalicky, J.; Kay, L.; Kern, D. *Nature* **2005**, *438*, 117−121.
(12) Boehr, D.; McElheny, D.; Dyson, H.; Wright, P. *Science* **2006**, *313*, 1638−1642.
(13) Henzler-Wildman.; et al. *Nature* **2007**, *450*, 838−844.
(14) Bruice, T. *Acc. Chem. Res.* **2002**, *35*, 139−148.
(15) Falzone, C.; Wright, P.; Benkovic, S. *Biochemistry* **1994**, *33*, 439−442.
(16) Osborne, M.; Schnell, J.; Benkovic, S.; Dyson, H.; Wright, P. *Biochemistry* **2001**, *40*, 9846−9859.
(17) Villa, J.; Warshel, A. *J. Phys. Chem. B* **2001**, *105*, 7887−7907.
(18) Warshel, A. *J. Biol. Chem.* **1998**, *273*, 27035−27038.
(19) Cui, Q.; Elstner, M.; Karplus, M. *J. Phys. Chem. B* **2002**, *106*, 2721−2740.
(20) Hansson, T.; Nordlund, P.; Åqvist, J. *J. Mol. Biol.* **1997**, *265*, 118−127.
(21) Warshel, A.; Sharma, P.; Kato, M.; Xiang, Y.; Liu, H.; Olsson, M. *Chem. Rev.* **2006**, *106*, 3210.
(22) Kienhöfer, A.; Kast, P.; Hilvert, D. *J. Am. Chem. Soc.* **2003**, *125*, 3206−3207.
(23) Lyne, P.; Mulholland, A.; Richards, W. *J. Am. Chem. Soc.* **1995**, *117*, 11345−11350.
(24) Shurki, A.; Štrajbl, M.; Villa, J.; Warshel, A. *J. Am. Chem. Soc.* **2002**, *124*, 4097−4107.
(25) Strajbl, M.; Shurki, A.; Kato, M.; Warshel, A. *J. Am. Chem. Soc.* **2003**, *125*, 10228−37.
(26) Bruice, T.; Lightstone, F. *Acc. Chem. Res.* **1999**, *32*, 137−144.
(27) Bruice.; et al. *Biochemistry* **2000**, *39*, 6267.
(28) Schowen, R. *Proc. Natl. Acad. Sci. U.S.A.* **2003**, *100*, 11931−11932.
(29) Hur, S.; Bruice, T. *Proc. Natl. Acad. Sci. U.S.A.* **2003**, *100*, 12015−12020.
(30) Hur, S.; Bruice, T. *Proc. Natl. Acad. Sci. U.S.A.* **2002**, *99*, 1176−1181.
(31) Hur, S.; Bruice, T. *J. Am. Chem. Soc.* **2003**, *125*, 5964−5972.
(32) Ranaghan, K.; Mulholland, A. *Chem. Commun.* **2004**, 1238−1239.
(33) Guo, H.; Cui, Q.; Lipscomb, W.; Karplus, M. *Angew. Chem., Int. Ed.* **2003**, *42*, 1508−1511.
(34) Burgi, H.; Dunitz, J.; Shefter, E. *J. Am. Chem. Soc.* **1973**, *95*, 5065−5067.
(35) Bürgi, H.; Lehn, J.; Wipff, G. *J. Am. Chem. Soc.* **1974**, *96*, 1956−1957.
(36) Dunitz.; et al. *Tetrahedron* **1974**, *30*, 1563−1572.
(37) Burgi, H.; Dunitz, J.; Shefter, E. *Acta. Crystall. Sect. B* **1974**, *30*, 1517−1527.
(38) Prabu-Jeyabalan, M.; Nalivaika, E.; Schiffer, C. A. *J. Mol. Biol.* **2000**, *301*, 1207−1220.
(39) Prabu-Jeyabalan, M.; Nalivaika, E.; Schiffer, C. A. *Structure* **2002**, *10*, 369−381.
(40) Pietrucci, F.; Marinelli, F.; Carloni, P.; Laio, A. *J. Am. Chem. Soc.* **2009**, *131*, 11811−11818.
(41) Toth, G.; Borics, A. *Biochemistry* **2006**, *45*, 6606−6614.
(42) Ozen, A.; Haliloğlu, T.; Schiffer, C. A. *J. Mol. Biol.* **2011**, *410*, 726−44.

(43) Piana, S.; Carloni, P.; Parrinello, M. *J. Mol. Biol.* **2002**, *319*, 567−583.
(44) Piana, S.; Bucher, D.; Carloni, P.; Rothlisberger, U. *J. Phys. Chem. B* **2004**, *108*, 11139−11149.
(45) Hyland, L. J.; Tomaszek, T. A., Jr.; Meek, T. D. *Biochemistry* **1991**, *30*, 8454−8463.
(46) Piana, S.; Sebastiani, D.; Carloni, P.; Parrinello, M. *J. Am. Chem. Soc.* **2001**, *123*, 8730−8737.
(47) Wittayanarakul, K.; Hannongbua, S.; Feig, M. *J. Comput. Chem.* **2008**, *29*, 673−685.
(48) Torbeev, V. Y.; Raghuraman, H.; Hamelberg, D.; Tonelli, M.; Westler, W. M.; Perozo, E.; Kent, S. B. *Proc. Natl. Acad. Sci. U.S.A.* **2011**, *108*, 20982−20987.
(49) Wlodawer, A.; Vondrasek, J. *Annu. Rev. Biophys. Biomol. Struct.* **1998**, *27*, 249−284.
(50) Maschera, B.; Darby, G.; Palu, G.; Wright, L. L.; Tisdale, M.; Myers, R.; Blair, E. D.; Furfine, E. S. *J. Biol. Chem.* **1996**, *271*, 33231−33235.
(51) Radzicka, A.; Wolfenden, R. *J. Am. Chem. Soc.* **1996**, *118*, 6105−6109.
(52) Berman, H. M.; Westbrook, J.; Feng, Z.; Gilliland, G.; Bhat, T. N.; Weissig, H.; Shindyalov, I. N.; Bourne, P. E. *Nucleic Acids Res.* **2000**, *28*, 235−242.
(53) Kovalskyy, D.; Dubyna, V.; Mark, A. E.; Korenelyuk, A. *Proteins: Struct. Funct. Bioinf.* **2005**, *58*, 450−458.
(54) Park, H.; Suh, J.; Lee, S. *J. Am. Chem. Soc.* **2000**, *122*, 3901−3908.
(55) Duan, Y.; Wu, C.; Chowdhury, S.; Lee, M. C.; Xiong, G.; Zhang, W.; Yang, R.; Cieplak, P.; Luo, R.; Lee, T. *J. Comput. Chem.* **2003**, *24*, 1999−2012.
(56) Jorgensen, W. L.; Chandrasekhar, J.; Madura, J. D.; Impey, R. W.; Klein, M. L. *J. Chem. Phys.* **1983**, *79*, 926−935.
(57) Ryckaert, J. P.; Ciccotti, G.; Berendsen, H. J. C. *J. Comput. Phys.* **1977**, *23*, 327−341.
(58) Harvey, M.; De Fabritiis, G. *J. Chem. Theory Comput.* **2009**, *5*, 2371−2377.
(59) Essmann, U.; Perera, L.; Berkowitz, M. L.; Darden, T. *J. Chem. Phys.* **1995**, *103*, 8577−9593.
(60) Harvey, M. J.; Giupponi, G.; Fabritiis, G. D. *J. Chem. Theory Comput.* **2009**, *5*, 1632−1639.
(61) Sadiq, S. K.; Noé, F.; De Fabritiis, G. *Proc. Natl. Acad. Sci. U.S.A.* **2012**, *109*, 20449−20454.
(62) Buch, I.; Harvey, M. J.; Giorgino, T.; Anderson, D. P.; De Fabritiis, G. *J. Chem. Inf. Model.* **2010**, *50*, 397−403.
(63) Sadiq, S. K.; De Fabritiis, G. *Proteins* **2010**, *78*, 2873−2885.
(64) Hornak, V.; Abel, R.; Okur, A.; Strockbine, B.; Roitberg, A.; Simmerling, C. *Proteins: Struct. Funct. Bioinf.* **2006**, *65*, 712−725.
(65) Garrec, J.; Sautet, P.; Fleurat-Lessard, P. *J. Phys. Chem. B* **2011**, *115*, 8545−8558.
(66) Kovalevsky, A. Y.; Chumanevich, A. A.; Liu, F.; Louis, J. M.; Weber, I. T. *Biochemistry* **2007**, *46*, 14854−14864.
(67) Shaw, D. E.; Maragakis, P.; Lindorff-Larsen, K.; Piana, S.; Dror, R. O.; Eastwood, M. P.; Bank, J. A.; Jumper, J. M.; Salmon, J. K.; Shan, Y.; Wriggers, W. *Science* **2010**, *330*, 341−346.